TU Delft

Delft University of Technology

Equivalent Circuit Models of Finite Slot Antennas

van Schelven, Ralph M.; Cavallo, Daniele; Neto, Andrea

DOI
10.1109/TAP.2019.2908112

Publication date
2019

Document Version
Accepted author manuscript

Published in
IEEE Transactions on Antennas and Propagation

Citation (APA)
van Schelven, R. M., Cavallo, D., & Neto, A. (2019). Equivalent Circuit Models of Finite Slot Antennas. *IEEE Transactions on Antennas and Propagation*, *67*(7), 4367-4376. Article 8676262. https://doi.org/10.1109/TAP.2019.2908112

Important note
To cite this publication, please use the final published version (if applicable).
Please check the document version above.

Copyright
Other than for strictly personal use, it is not permitted to download, forward or distribute the text or part of it, without the consent of the author(s) and/or copyright holder(s), unless the work is under an open content license such as Creative Commons.

Takedown policy
Please contact us and provide details if you believe this document breaches copyrights.
We will remove access to the work immediately and investigate your claim.

This work is downloaded from Delft University of Technology.
For technical reasons the number of authors shown on this cover page is limited to a maximum of 10.

© 2019 IEEE. Personal use of this material is permitted. Permission from IEEE must be obtained for all other uses, in any current or future media, including reprinting/republishing this material for advertising or promotional purposes, creating new collective works, for resale or redistribution to servers or lists, or reuse of any copyrighted component of this work in other works.

Equivalent Circuit Models of Finite Slot Antennas

Ralph M. van Schelven, *Student Member, IEEE*, Daniele Cavallo, *Member, IEEE*, Andrea Neto, *Fellow, IEEE*

***Abstract*— We present a systematic approach to describe planar slot antennas, embedded in generic stratified media. An equivalent transmission line model for the slot is proposed, based on a spectral domain analysis. First, we introduce a method of moments solution to model semi-infinite or finite slots, fed by a delta-gap excitation. The solution entails only two basis functions, one located at the feed and the other at the termination. The latter basis function is chosen to properly account for the field diffractive behavior at the antenna end points. An approximate circuit model is then introduced, which describes the main mode propagating along the slot as an equivalent transmission line. Lumped impedances are extracted to accurately describe the source and the end points: the reactances account for the reactive nature of the feed and the termination, while the resistances represent the radiated space waves, emerging from both the feed and the end points. This procedure can be used to derive the input impedance of planar slot antennas with arbitrary length in generic layered media or the interaction between multiple feeds within the same slot.**

***Index Terms*—Equivalent circuit, input impedance, slot antenna.**

I. Introduction

PRINTED slot antennas are among the most common planar antennas in use today and have been studied extensively in the literature, both as isolated elements and in array configurations. Their structure is complementary to the printed dipoles, thus all known analytical solutions of canonical dipole antennas can be applied also to slots by using Babinet's principle [1]. However, realistic slot antennas are not radiating in free-space but in the presence of a more complex dielectric stratification. In these cases, the input impedance is typically determined with general-purpose numerical methods.

A convenient way to describe a center-fed slot is by an equivalent transmission line, where the excitation is modeled as a shunt generator and the slot arms are represented as two transmission line sections. For example, equivalent transmission line models were used in [2]–[4] to aid the design of slot antennas with different loadings. To compute the characteristic impedance and the propagation constant of the slot lines, different methods have been proposed in [5]–[8]. Several transmission line models for slot antennas are based on the solutions given in [9], [10]. In particular, the approach in [9] was based on equating the power radiated by the slot to the power delivered to a lossy transmission line. Moreover, both the models in [9], [10] considered short circuits to describe the slot terminations, thus did not account for the reactance associated with the end points. An improved model was proposed in [11], where the inductance of the slot shorted ends was considered.

A limit of all the mentioned models of finite slot antennas is that they do not account for the reactance of the feed and the diffraction from the edges. Besides, the radiation is modeled as a distributed resistance through a lossy line or as a single lumped resistance, thus it is not possible to separate the contributions to the radiated power that are emerging from the feed and from the end points.

A different approach is presented here, where an improved model is proposed that accurately describes the reactive nature of both the feed and the terminations of the slot. First, a Method of Moments (MoM) solution is given where, by using the Green's function of an infinite slot [12], only two basis functions are employed to describe the current in the feeding gap and at the edges of the antennas. The basis functions are appropriately chosen to represent the reactance due to the finite dimension of the feed and due to the diffraction of the electromagnetic field at the end points. Moreover, the MoM solution allows representing the radiation from the slot in terms of three separate resistances, one associated with the feed point and two located at the edges. Such configuration gives more physical insight, as the radiated field can be interpreted as three space waves, emerging from the feed and the end points.

An additional advantage of the proposed method is that the characteristic impedance of the transmission line is derived by extracting the polar singularity contribution of the spectral domain Green's function as in [13], [14], thus can be generalized to arbitrary stratified media, as long as the polar and the branch singularity do not coincide.

This paper is structured as follows: in Sec. II, we discuss the MoM solution for semi-infinite slots, by starting with the spectral magnetic current distribution on an infinite slot and then introducing the termination. Subsequently, in Sec. III, an equivalent circuit of the slot is provided, based on the numerical solution. The model is extended to represent finite slots in Sec. III-D. The physical phenomena near the termination of the slot are studied in Sec. IV, by quantifying the end-point impedance, the power launched in quasi-TEM waves propagating along the slot, as well as the power radiated as space waves, followed by conclusions in Sec. V.

II. MoM Solution for Semi-Infinite Slot

This section describes the steps for calculating the input impedance and the current distribution of a semi-infinite slot

Manuscript received Month DD, YYYY; revised Month DD, YYYY; accepted Month DD, YYYY. Date of publication Month DD, YYYY; date of current version Month DD, YYYY. This work was supported by the Netherlands Organization for Scientific Research (NWO) TTW-NXP Partnership Program Project no. 15591. *(Corresponding author: Ralph M. van Schelven)*

The authors are with the Microelectronics Department, Delft University of Technology, 2628 CD Delft, The Netherlands (e-mail: r.m.vanschelven@tudelft.nl).

Color versions of one or more of the figures in this communication are available online at http://ieeexplore.ieee.org.

Digital Object Identifier XX.XXXX/TAP.XXXX.XXXXXXXX.

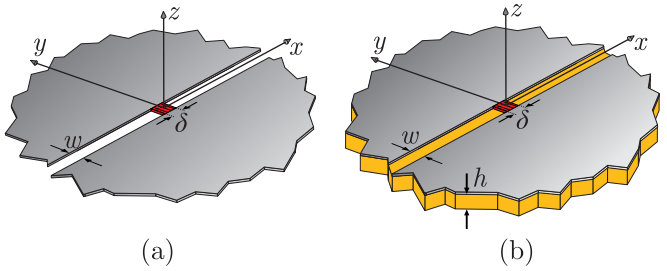

Fig. 1. Infinite slot (a) in free-space and (b) printed on a dielectric slab.

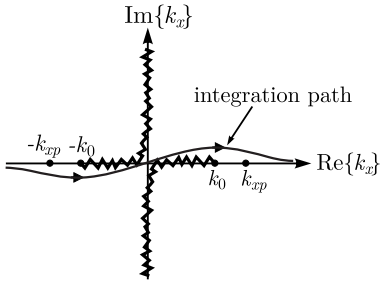

Fig. 2. Branch cuts and poles in the complex k_x-plane for a slot with a thin dielectric substrate. The deformed integration path to avoid the singularities is also shown.

in an arbitrary stratification. The infinite slotline solution is given first, as it constitutes the basis for the theory described in the remainder of the paper. The termination of the slot is then introduced and described by means of an ad-hoc basis function that accounts for the diffraction at the slot edge.

A. Infinite Slot

Let us consider an infinite slot oriented along x in the presence of a generic dielectric stratification. For example, the slot can be in free-space, as shown in Fig. 1(a), or printed on a dielectric slab, as in Fig. 1(b). The slot is assumed to be electrically narrow and excited by a feeding gap, which is small in terms of wavelength (δ-gap excitation). The solution for the voltage along the slot can be written as a one-dimensional inverse Fourier transform, similar to [13, eq. (1)]:

$$v(x) = \frac{1}{2\pi}\int_{-\infty}^{\infty} \frac{i_\delta F_\delta(k_x)}{D_s(k_x)} e^{-jk_x x} dk_x \tag{1}$$

where i_δ is the average current in the feeding gap, $F_\delta(k_x)$ is the spectral basis function representing the difference between the impressed tangential magnetic fields above and below the slot plane, exciting the gap:

$$F_\delta(k_x) = \text{sinc}\left(\frac{k_x\delta}{2}\right) \tag{2}$$

and

$$D_s(k_x) = \frac{1}{2\pi}\int_{-\infty}^{\infty} G_{xx}^{hm}(k_x,k_y) M_t(k_y) dk_y \tag{3}$$

is the spectral longitudinal Green's function of an infinite slot, defined in [12, eq. (8)]. G_{xx}^{hm} is the xx-component of the spectral dyadic Green's function relating magnetic field to magnetic source, and k_x and k_y are the spectral counterparts of the spatial variables x and y, respectively. As the transverse current distribution is assumed to be edge-singular, its Fourier transform is the zeroth order Bessel function of the first kind $M_t(k_y) = -J_0(k_y w/2)$. The integral in (3) can be solved analytically for free-space or for slots at the interface between two homogeneous media [12], while it can be computed numerically for generic stratification.

The input impedance of the infinite slot can be defined as the ratio of the average voltage (v_δ) and the average current (i_δ) over the feeding gap:

$$Z_{\text{in}} = \frac{v_\delta}{i_\delta} = \frac{\frac{1}{\delta}\int_{-\delta/2}^{\delta/2} v(x)dx}{i_\delta}. \tag{4}$$

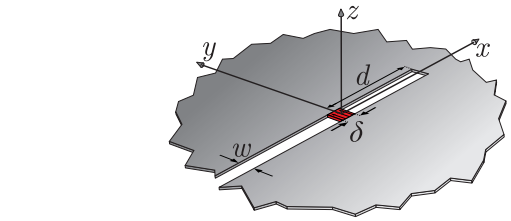

Fig. 3. Semi-infinite slot in free-space.

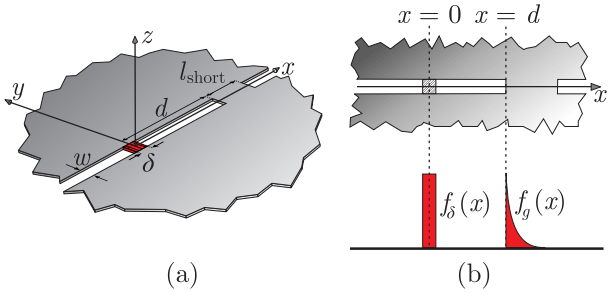

Fig. 4. (a) Interrupted infinite slot in free-space; (b) Space domain basis functions with respect to their location along the semi-infinite slot.

By substituting (1) in (4) and evaluating the integral in dx, the input impedance can be expressed as a single spectral integral:

$$Z_{\text{in}} = \frac{1}{2\pi}\int_{-\infty}^{\infty} \frac{F_\delta(k_x)F_\delta(-k_x)}{D_s(k_x)} dk_x\,. \tag{5}$$

The integrands in (1) and (5) present square-root branch and polar singularities. The location of these singularities in the complex plane depends on the layered dielectric medium under consideration. For example, for the geometry in Fig. 1(b), the branch points are in $k_x = \pm k_0$ and the poles are in $k_x = \pm k_{xp}$, as shown in Fig. 2. The integrals can be then solved numerically along the deformed path also shown in the figure.

B. Semi-Infinite Slot

Let us now consider a semi-infinite slot, interrupted at a certain distance, d, from the feeding gap, as depicted in Fig. 3. A convenient way to represent the semi-infinite slot is to assume that the short is realized with a metallic interruption of finite length l_{short}, as shown in Fig. 4(a). The length of the short is sufficiently large so that the magnetic current induced

in the slot for $x > d + l_{\text{short}}$ does not influence the current at $x < d$. This assumption allows modeling a semi-infinite slot with infinitely extended metal (for $x > d$) as an infinite slot with a finite metal termination. Such an approximation is beneficial due to the availability of the infinite slot spectral Green's function in (3).

To represent the boundary conditions on the shorted end, an electric current is assumed to be distributed at $x > d$ with an edge-singular behavior, as shown in Fig. 4(b). The edge-singular behavior is assumed to be represented with the following basis function:

$$f_g(x) = \frac{2}{g\pi}\left(\frac{\text{rect}_{g/2}(x-(d+g/4))}{\sqrt{1-\left(\frac{2(x-(d+g/2))}{g}\right)^2}} - 1\right) \tag{6}$$

where $\text{rect}_l(x)$ is equal to 1 for $x \in [-l/2, l/2]$ and 0 elsewhere, and the parameter g in (6) is related to the width of the current distribution on the metallic interruption. The choice of the value for g is found to be linked to the width of the slot and the free-space wavelength λ as

$$g = \frac{5}{3}\sqrt{w\lambda}\,. \tag{7}$$

The expression for g has been derived empirically by curve fitting the numerical data obtained with a parametric analysis performed in CST. The accuracy of this expression will be later assessed by comparing our results for the slot input impedance with commercial electromagnetic solvers.

With the given choice of the basis functions, the voltage on the semi-infinite slot can be expressed similarly to (1) as follows [15, eq. (19)]:

$$v(x) = \frac{1}{2\pi}\int_{-\infty}^{\infty} \frac{i_\delta F_\delta(k_x) + i_g F_g(k_x)}{D_s(k_x)} e^{-jk_x x} dk_x \tag{8}$$

where i_g is the average current on the metallic interruption and $F_g(k_x)$ is the Fourier transform of (6), which can be calculated in closed form as

$$F_g(k_x) = e^{jk_x g/2} \times \left(J_0\left(\frac{k_x g}{2}\right) - j\mathbf{H}_0\left(\frac{k_x g}{2}\right) - \frac{2}{\pi}\text{sinc}\left(\frac{k_x g}{4}\right)e^{-jk_x g/4}\right) \tag{9}$$

with $\mathbf{H}_0$ being the zeroth order Struve function.

The average voltage on the delta-gap feed (v_δ) and on the metallic interruption (v_g) can be expressed by Galerkin projection of (8) on the corresponding basis functions, which after some algebraic manipulations yields the following system of two linear equations [15, eq. (17)]:

$$\begin{cases} v_\delta = i_\delta Z_{\delta\delta} + i_g Z_{\delta g} \\ v_g = i_\delta Z_{g\delta} + i_g Z_{gg} = 0 \end{cases} \tag{10}$$

where we imposed $v_g = 0$ for the perfect conducting termination. The mutual and self-impedances are given by

$$Z_{ji} = \frac{1}{2\pi}\int_{-\infty}^{\infty} \frac{F_i(k_x)F_j(-k_x)e^{jk_x(x_i - x_j)}}{D_s(k_x)} dk_x \tag{11}$$

where the subscripts i and j can refer to either δ or g, and the locations of the basis functions are defined as $x_\delta = 0$ and $x_g = d$. The input impedance of the slot can now be derived from (10) as the ratio between the average voltage and the current on the delta-gap:

$$Z_{\text{in,MoM}} = \frac{v_\delta}{i_\delta} = Z_{\delta\delta} - \frac{Z_{\delta g}Z_{g\delta}}{Z_{gg}}\,. \tag{12}$$

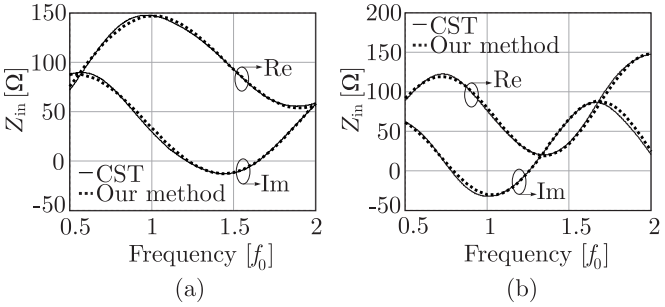

Fig. 5. Comparison between the input impedance of a semi-infinite slot calculated with our method and CST for a slot (a) in free-space and (b) with a thin dielectric slab. The geometrical parameters of the structure are $d = \lambda_0/4$, $w = \lambda_0/50$ and $\delta = \lambda_0/40$, where λ_0 is the wavelength in free-space at f_0. The dielectric substrate is characterized by $\varepsilon_r = 4$, $h = \lambda_d/20$ when λ_d is the wavelength in the dielectric at f_0.

As a numerical example, Fig. 5(a) shows the input impedance of a semi-infinite slot in free-space calculated as described above, compared to CST. The distance between the excitation gap and the termination of the slot is $d = \lambda_0/4$, the width of the slot is $w = \lambda_0/50$ and the length of the delta-gap is $\delta = \lambda_0/40$, where λ_0 is the wavelength in free-space at the frequency f_0. Figure 5(b) shows the input impedance of the same semi-infinite slot, when a thin dielectric substrate is added. The relative permittivity of the dielectric is $\varepsilon_r = 4$ and the height of the slab is $h = \lambda_d/20$, where λ_d is the wavelength in the dielectric at f_0. A very good agreement is observed in both examples.

III. Equivalent Transmission Line Circuit

Based on the numerical solution, an equivalent circuit model can be derived. The procedure entails the analysis of the polar and branch singularities of the spectral integral expressions of the impedances. The pole contributions to the integrals, when solved with the residue theorem, can be represented with equivalent transmission lines describing the guided propagation along the slot.

A. Residue Contribution of the Input Impedance of an Infinite Slot

The integrand in the impedance expression in (5) presents two types of singularities that can be recognized by writing the denominator $D_s(k_x)$ explicitly: square-root branch points, representing radiated space waves, and poles associated with quasi-TEM waves guided along the slot. When the poles and the branch points coincide, e.g. for a slot on perfectly conducting plane radiating in a homogeneous medium, the two contributions cannot be considered separately. In these cases, the integral in (5) can be solved asymptotically with the method in [16]. This approach allows writing the voltage on

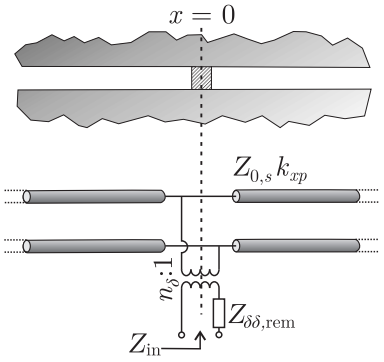

Fig. 6. Equivalent transmission line of an infinite slot.

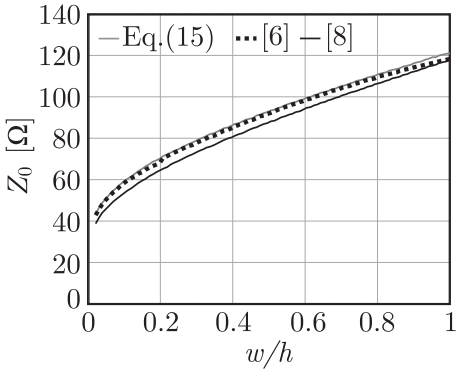

Fig. 7. Comparison between the characteristic impedance of a slotline in the presence of a dielectric slab with $h = \lambda_0/40$ and $\varepsilon_r = 10$. The characteristic impedance is shown as a function of the ratio between w and h.

the slot for large values of $(x_i - x_j)$ as the solution of a tapered transmission line with x-dependent characteristic impedance, which is, however, not convenient to model multiple feed points or terminations.

To isolate the polar contribution from the branch, one can introduce small losses in the ground plane [13], [17] or a thin dielectric substrate, so that the pole singularity moves away from the branch point in the complex k_x-plane. The location of the pole, k_{xp}, can be found using a local-search algorithm (e.g. Newton's method) starting from an appropriate initial point.

By using Cauchy's residue theorem, the polar contributions of the input impedance of an infinite slot defined in (5) can be written as

$$Z_{\delta\delta,\mathrm{TL}} = -j\frac{F_\delta(k_{xp})F_\delta(-k_{xp})}{D_s'(k_{xp})} = -j\frac{F_\delta(-k_{xp})^2}{D_s'(k_{xp})} \qquad (13)$$

where the prime $(')$ indicates the operation of differentiation.

By representing the impedance as two parts, namely its residual contribution and a remaining term as

$$Z_{\mathrm{in}} = Z_{\delta\delta,\mathrm{TL}} + Z_{\delta\delta,\mathrm{rem}} \qquad (14)$$

the infinite slot can be represented by an equivalent circuit, as shown in Fig. 6. The model consists of two semi-infinite transmission line sections representing the slotline and a transformer with turn ratio $n_\delta = F_\delta(-k_{xp})$, in series with the impedance $Z_{\delta\delta,\mathrm{rem}}$. The characteristic impedance of the transmission line is given by [13, eq. (7)]

$$Z_{0,s} = -\frac{2j}{D_s'(k_{xp})}\,. \qquad (15)$$

Figure 7 shows a comparison between the characteristic impedance of the transmission line calculated with (15) and the methods described in [6] and [8]. The characteristic impedance is calculated for a slotline in the presence of a dielectric slab of height $h = \lambda_0/40$ and a relative permittivity equal to $\varepsilon_r = 10$, for the sake of comparison with [6, eq. (3) and (5)] and [8, eq. (7)]. It can be seen that the characteristic impedance as a function of the ratio between w/h corresponds well to the values found in previously published literature.

The resistance and reactance representing the radiation emanating from the feed and the reactive energy around the feed respectively, are represented as a lumped impedance, $Z_{\delta\delta,\mathrm{rem}}$. This impedance is compared to values extracted from

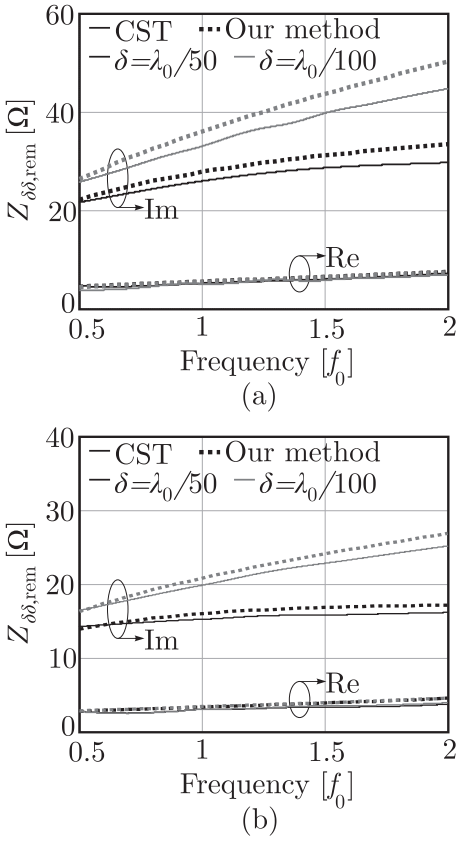

Fig. 8. Comparison between the lumped impedance $Z_{\delta\delta,\mathrm{rem}}$ as found using our method and extracted from CST. The slot is in the presence of a slab with $h = \lambda_d/20$ and $\varepsilon_r = 4$. The impedances are shown for $\delta = \lambda_0/50$ and for $\delta = \lambda_0/100$. (a) $w = \lambda_0/50$. (b) $w = \lambda_0/100$.

CST in Fig. 8, by calculating the input impedance of an infinite slot, and subtracting $Z_{\delta\delta,\mathrm{TL}}$ as calculated with (13). The height of the dielectric slab is $h = \lambda_d/20$ and the relative permittivity of the material is $\varepsilon_r = 4$. The value for $Z_{\delta\delta,\mathrm{rem}}$ is shown for $\delta = \lambda_0/50$ and for $\delta = \lambda_0/100$ both for $w = \lambda_0/50$ in Fig. 8(a) and for $w = \lambda_0/100$ in Fig. 8(b). It can be seen that the real part of the impedance does not depend on the length of the gap. The reactance calculated with our method is slightly lower than the reactance found from CST. This difference is larger

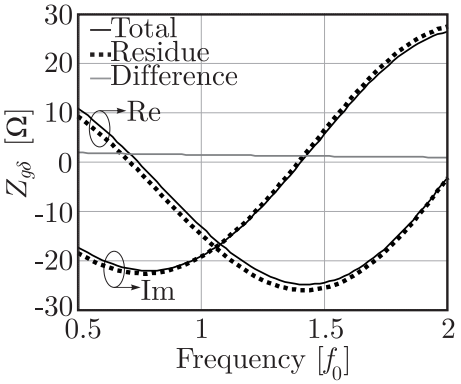

Fig. 9. Comparison between the total mutual impedance $Z_{g\delta}$ and the contribution due to the residue as a function frequency. The geometrical parameters are set to: $d = \lambda_0/4$, $w = \lambda_0/50$, $\delta = \lambda_0/40$, $\lambda_d/20$ and $\varepsilon_r = 4$.

for wider slots and can be explained by the approximation of electrically narrow slots used to define $D_s(k_x)$ in (3).

B. Residue Contribution of the Mutual Impedance

Similarly, by using the residue theorem, the polar contributions of the mutual impedance $Z_{g\delta}$, defined in (11), can be written as

$$Z_{g\delta,\mathrm{TL}} = -j\frac{F_\delta(k_{xp})F_g(-k_{xp})}{D_s'(k_{xp})}e^{-jk_{xp}d}\,. \tag{16}$$

Figure 9 shows the comparison between the total integral $Z_{g\delta}$ and the contribution due to the residue $Z_{g\delta,\mathrm{TL}}$, as a function of frequency. The slot under consideration is printed on a dielectric slab. It can be seen that the difference between the total mutual impedance and the residue contribution ($|Z_{g\delta} - Z_{g\delta,\mathrm{TL}}|$) decreases with the frequency, since the distance between the two basis functions becomes larger in terms of the wavelength. This effect can be interpreted by noting that, for small distances, the interaction between the feed and the termination is not only described by the propagating mode (residue) but also by space-wave coupling. For larger distance, the space wave contribution is less important, due to its geometrical spreading, thus the residue component, which has no spreading, becomes dominant.

By approximating the mutual impedance with its residual contribution, the equivalent model introduced for infinite slots can be extended to semi-infinite slots as shown in Fig. 10(a). An additional impedance transformer is included at the termination of the slot with turn ratio $n_g = F_g(-k_{xp})$. Similarly to (13) and (14), we can define the contribution of the transmission line to the self-impedance of the edge basis function as

$$Z_{gg,\mathrm{TL}} = \frac{1}{2}Z_{0,s}n_g^2 = -j\frac{F_g(-k_{xp})^2}{D_s'(k_{xp})} \tag{17}$$

and the remaining contribution to the total self-impedance as

$$Z_{gg,\mathrm{rem}} = Z_{gg} - Z_{gg,\mathrm{TL}}\,. \tag{18}$$

The length of the transmission line section separating the two transformers is equal to the distance between the feeding point and the metallic interruption (d).

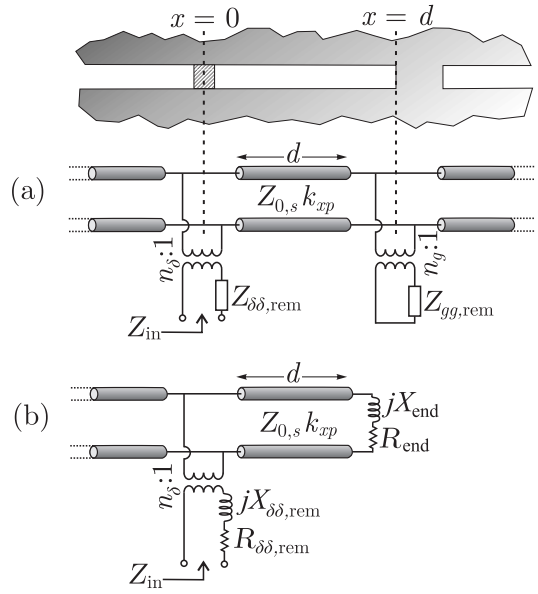

Fig. 10. Equivalent transmission line of the semi-infinite slot: (a) transformers and impedances associated with the feeding point and the termination, in parallel to an infinite line; (b) lumped equivalent termination impedance.

We can also define a single lumped impedance to represent the end point as

$$Z_{\mathrm{end}} = \frac{\left(Z_{gg,\mathrm{rem}}/n_g^2\right)Z_{0,s}}{\left(Z_{gg,\mathrm{rem}}/n_g^2\right) + Z_{0,s}} = R_{\mathrm{end}} + jX_{\mathrm{end}}\,. \tag{19}$$

The end-point impedance can be represented as a resistor accounting for radiation and an inductor accounting for the reactive energy at the termination, such that the equivalent circuit of the semi-infinite slot becomes as in Fig. 10(b).

C. Input Impedance and Accuracy of the Circuit Model

The input impedance of the slot can be found from the circuit as

$$Z_{\mathrm{in,TL}} = Z_{\delta\delta,\mathrm{rem}} + n_\delta^2\frac{Z_{\mathrm{end}}^{\mathrm{rep}}Z_{0,s}}{Z_{\mathrm{end}}^{\mathrm{rep}} + Z_{0,s}} \tag{20}$$

where

$$Z_{\mathrm{end}}^{\mathrm{rep}} = Z_{0,s}\frac{Z_{\mathrm{end}} + jZ_{0,s}\tan(k_{xp}d)}{Z_{0,s} + jZ_{\mathrm{end}}\tan(k_{xp}d)}\,. \tag{21}$$

Figure 11 shows the comparison between the input impedance of a semi-infinite slot in free-space calculated using the previously introduced method of moments and with the transmission line model. The distance between the end point of the slot and the feeding gap $d = \lambda_0/4$, the width of the slot is $w = \lambda_0/90$ and the length of the feeding gap is $\delta = \lambda_0/90$. Two different conductivities of the ground plane are considered: $\sigma = 6 \times 10^7$ S/m (copper) and $\sigma = 1000$ S/m. The corresponding distances between k_{xp} and k_0 are $0.0003k_0$ and $0.11k_0$, respectively, as shown in the figure. It can be seen that for $\sigma = 6\times10^7$ S/m the transmission line does not describe the input impedance accurately, as the distance between the pole k_{xp} and the branch point k_0 in the complex k_x-plane is too small to separate the two contributions. In the case when $\sigma = 1000$ S/m this distance is larger, thus the polar

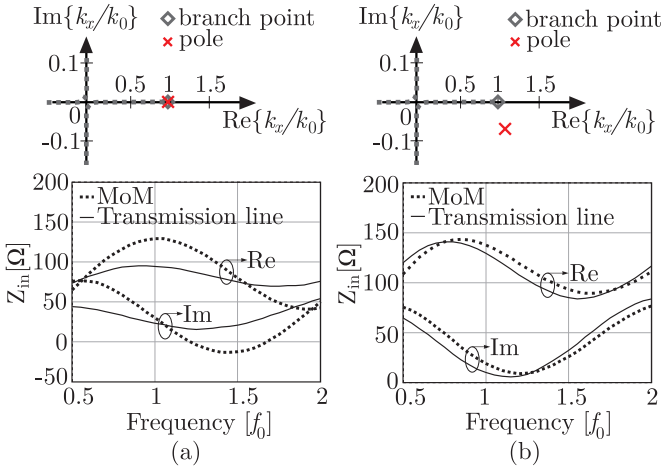

Fig. 11. Comparison between the input impedance of a semi-infinite slot in a lossy ground plane calculated with our method and CST for (a) $\sigma = 6\times10^7$ S/m and (b) $\sigma = 1000$ S/m. The geometrical parameters of the structure are $d = \lambda_0/4$, $w = \lambda_0/90$ and $\delta = \lambda_0/90$. The locations of the pole with respect to the branch point are also shown.

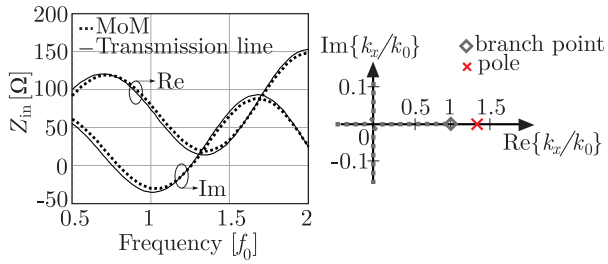

Fig. 12. Comparison between the input impedance of a semi-infinite slot on a dielectric substrate calculated with the transmission line model and the MoM. The geometrical parameters of the structure are $d = \lambda_0/4$, $w = \lambda_0/50$, $\delta = \lambda_0/40$, $h = \lambda_d/20$ and $\varepsilon_r = 4$. The location of the pole with respect to the branch point is also shown.

contribution can be extracted and represents the wave launched along the slot better.

Figure 12 shows a similar comparison when a small dielectric is introduced. The dimensions of the structure are the same as in Fig. 5(b). The presence of a thin dielectric is an effective way to separate the space wave and the guided wave contributions. Indeed, a good accuracy of the equivalent transmission line model can be observed in Fig. 12, as the distance between k_{xp} and k_0 is $0.34k_0$ at $f = f_0$.

As pointed out earlier, the accuracy of the equivalent transmission line model depends on the distance d between the feed and the end point. This dependence can be explained by the space-wave interaction between the two basis functions, that is not accounted for in the transmission line model. The space-wave coupling can be comparable to the guided-wave interaction for small distances, but its effect has less and less impact as the distance increases, due to the spherical spreading of the space wave. To highlight this effect, Fig. 13 shows the relative error of the input impedance of a semi-infinite slot calculated with the transmission line circuit, as a function of the distance d, for three values of the width w. The relative

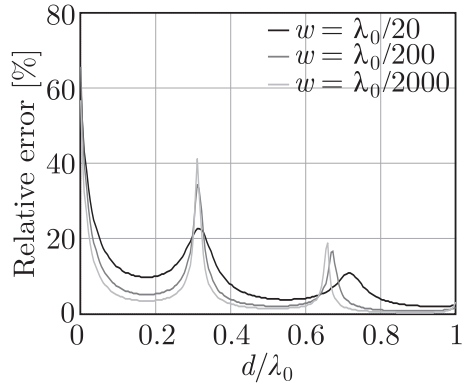

Fig. 13. Relative error with respect to the input impedance for the transmission line circuit, representing a semi-infinite slot on a thin dielectric substrate, as a function of the distance between the feeding point and the end of the slot, d. The length of the feeding gap is $\delta = \lambda_0/40$. The relative permittivity of the dielectric is $\varepsilon_r = 4$ and the height of the slab is $h = \lambda_d/20$.

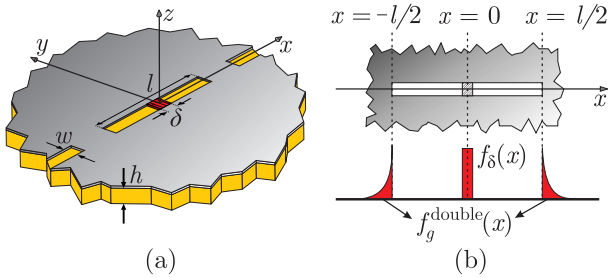

Fig. 14. (a) Finite slot on a dielectric substrate and (b) space domain basis functions with respect to their location along the finite slot.

error is defined as

$$\epsilon_{\text{rel}} = \frac{|Z_{\text{in,MoM}} - Z_{\text{in,TL}}|}{|Z_{\text{in,MoM}}|} \times 100\% \,. \tag{22}$$

The slot has a feeding gap with size $\delta = \lambda_0/40$ and is printed on a thin dielectric substrate, with height $h = \lambda_d/20$ and relative permittivity $\varepsilon_r = 4$. It can be seen that the relative error decreases as a function of the distance. The periodic peaks in the relative error correspond to minima in the impedance, with values that are close to zero, thus in these points small absolute errors correspond to high relative errors. Moreover, narrower slots yield smaller errors, because of reduced radiation associated with the basis functions and more dominant guiding effect along the slot.

D. Finite Slot

When considering a finite slot, as depicted in Fig. 14(a), the edge-singular electric current is induced on both metallic interruptions. For a center-fed finite slot, the MoM solution can be then derived in the same way as for the semi-infinite slot, by replacing the edge basis function $f_g(x)$ with a pair of such basis functions at the two edges $f_g^{\text{double}}(x)$, as shown in Fig. 14(b). Due to symmetry, the two edge-singular currents at the edges have the same amplitude, thus the basis functions can be written in the spectral domain as:

$$F_g^{\text{double}}(k_x) = F_g\left(k_x\right) e^{jk_x l/2} + F_g\left(-k_x\right) e^{-jk_x l/2} \tag{23}$$

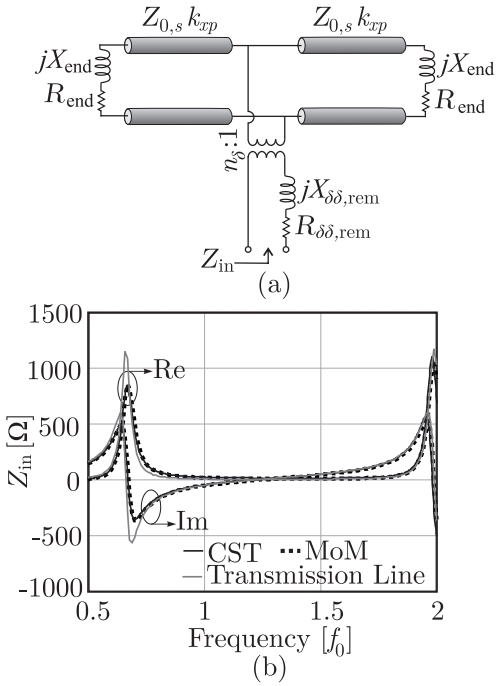

Fig. 15. (a) Equivalent transmission line circuit representing a finite slot. (b) Comparison between the input impedance of a finite slot in the presence of a dielectric substrate calculated with the transmission line model, our MoM and CST. The geometrical parameters of the structure are $l = \lambda_0/2$, $w = \lambda_0/50$, $\delta = \lambda_0/40$, $\varepsilon_r = 4$, $h = \lambda_d/20$.

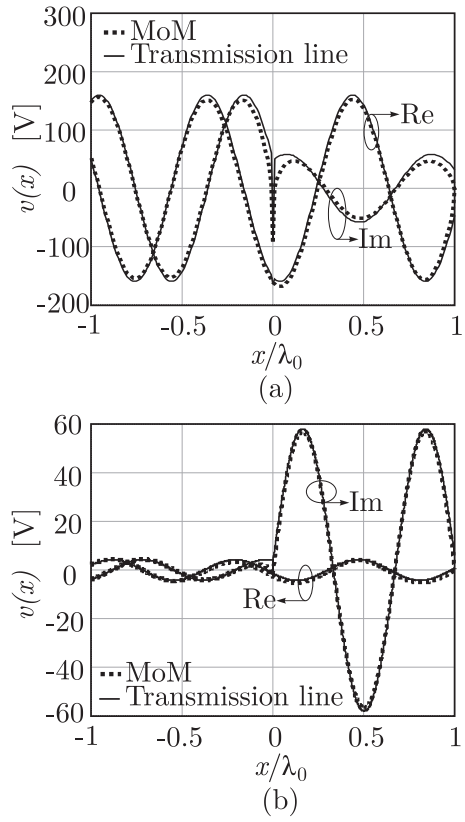

Fig. 16. Comparison between the voltage along a semi-infinite slot on a dielectric substrate calculated with the transmission line model and the MoM, for slot of width (a) $w = \lambda_0/20$ and (b) $w = \lambda_0/2000$. The excitation current is $i_\delta = 1$A, the geometrical parameters of the structure are $d = \lambda_0$, $\delta = \lambda_0/500$, $h = \lambda_d/20$ and $\varepsilon_r = 4$.

where l is the length of the slot. Following the procedure described earlier, the equivalent transmission line model for the finite slot becomes the one in Fig. 15(a). If the two arms of the slot are equal, the input impedance of the slot can be found from the circuit as

$$Z_{\text{in}} = Z_{\delta\delta,\text{rem}} + n_\delta^2 \frac{1}{2} Z_{\text{rep}}^{\text{end}} \tag{24}$$

where $Z_{\text{rep}}^{\text{end}}$ is defined in (21). Figure 15(b) shows the input impedance of a finite slot in the presence of a dielectric substrate calculated, comparing our MoM solution, a CST simulation and the equivalent transmission line model. The length of the slot is $l = \lambda_0/2$, the width of the slot is $w = \lambda_0/50$ and the length of the delta-gap is $\delta = \lambda_0/40$. The relative permittivity of the dielectric is $\varepsilon_r = 4$ and the height of the substrate is $h = \lambda_d/20$. A very good agreement between the MoM and CST is observed. The transmission line model also describes the resonance frequencies and the values of the impedance well. The accuracy of the approximated transmission line model is better for higher frequency, for which the electrical distance between the feed and the slot ends is larger.

IV. Analysis of the Slot Termination

In the previous sections an impedance has been introduced, which describes the end point of the slot. A more detailed analysis of the characteristic behavior of the fields close to the termination is presented in this section, with the aim to provide more physical insight to the reactive and radiative nature of the end point as a function of the slot width.

A. Voltage Distribution on the Slot

To this purpose, Fig. 16 shows the voltage along the semi-infinite slot calculated with the MoM and with the transmission line circuit. For example, we assume that the feeding gap is centered at $x = 0$, the termination is located at $x = \lambda_0$ and the slot is infinitely extended for $x < 0$. Two cases are considered for the slot width: $w = \lambda_0/20$ in Fig. 16(a) and $w = \lambda_0/2000$ in Fig. 16(b), with λ_0 being the wavelength at the calculation frequency f_0. In the transmission line, the voltage along the line is described by the sum of two forward and backward traveling sine waves, while in the MoM solution the voltage is given by (8). Clear differences can be seen between the two methods in the proximity of the feeding gap and the end point, for the larger slot width in Fig. 16(a). The voltage calculated using the transmission line model is not zero at the end point, but equal to the voltage across the load Z_{end}. On the contrary, the voltage calculated with the MoM goes to zero at the end point, but it deviates from the sinusoidal distribution close to the termination. For the narrower slot in Fig. 16(b), the discrepancy near the discontinuities is much less apparent.

The deviation from the sine profile can be explained by observing the real field distribution on the slot, evaluated with a three-dimensional full-wave method. The electric field along the slot is oriented in the transverse direction, as the tangential component of the electric field on a perfect electric conductor

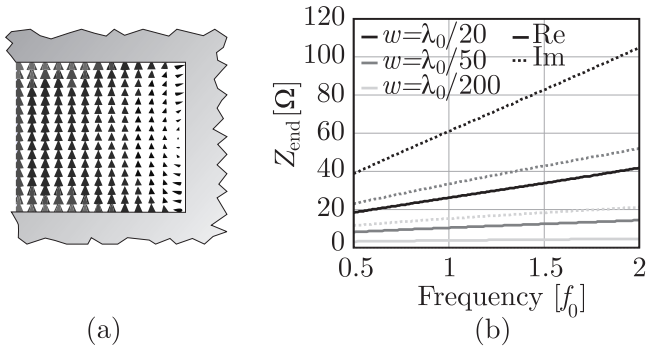

Fig. 17. (a) Electric field vector lines inside a semi-infinite slot near the end point; (b) Values of the end-point impedance Z_{end} as a function of frequency for three different widths of a semi-infinite slot on a dielectric substrate. The height of the substrate is $h = \lambda_d/40$ and the relative permittivity is $\varepsilon_r = 4$.

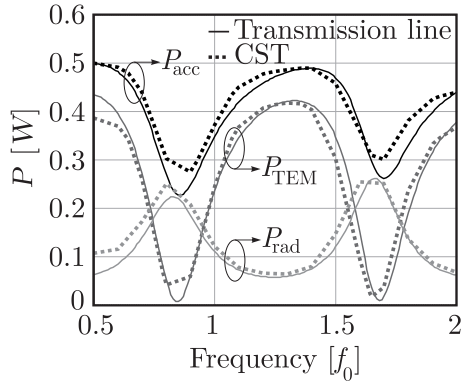

Fig. 18. Comparison between the radiated power and the power launched into the semi-infinite slotline calculated with the equivalent circuit and CST. The geometrical parameters are: $w = \lambda_0/50$, $\delta = \lambda_0/40$, $d = 0.45\lambda_0$, $h = \lambda_d/20$, $\varepsilon_r = 4$ and $Z_{\text{gen}} = 100\Omega$.

must be zero. However, near the end of the slot, the field lines bend in order to be normal to the metal on all three sides. This effect can be observed in Fig. 17(a), which depicts the vector field lines near the edge, calculated in CST. Since the magnetic current (or the voltage) along the slot is orthogonal to the electric field, the magnetic current also bends. This bending is more significant for wider slots and gives rise to a reactive field concentrated around the termination, as well as space waves radiated in all directions.

For very narrow slots, the voltage near the end point follows the sinusoidal behavior more closely, i.e. the voltage reflection coefficient at the termination is closer to -1 and the end-point impedance is more similar to a short circuit. Figure 17(b) shows the value of Z_{end} for different slot widths. It can be seen that, indeed, both the inductance and the radiation resistance associated with the end point decrease for narrower slots.

B. Power Balance

The transmission line circuit can be used to find the power radiated from the feeding gap and from the end point of the slot, as well as the power launched in the semi-infinite slotline. The radiated power, P_{rad}, is found as the sum of the power dissipated in $R_{\delta\delta,\text{rem}}$ and R_{end}, while the power launched along the slotline in the form of a quasi-TEM wave is indicated as P_{TEM}. In order to compare the values of radiated power calculated with our circuit and with CST, a constant power equal to 0.5 W is fed to the structure by a generator with an internal impedance Z_{gen}. The accepted power, entering the circuit, can be found as

$$P_{\text{acc}} = 0.5(1 - |S_{11}|^2) = P_{\text{rad}} + P_{\text{TEM}} \tag{25}$$

where $S_{11} = (Z_{\text{in}} - Z_{\text{gen}})/(Z_{\text{in}} + Z_{\text{gen}})$. Figure 18 shows the comparison of the power balance calculated with the circuit and from CST, showing a good agreement. The structure under consideration is a semi-infinite slot, on a thin dielectric slab, with parameters $w = \lambda_0/50$, $\delta = \lambda_0/40$, $d = 0.45\lambda_0$, $h = \lambda_d/20$ and relative permittivity of the dielectric $\varepsilon_r = 4$. The generator impedance is equal to $Z_{\text{gen}} = 100\Omega$. It can be noted that the power launched in the semi-infinite slot is maximum at the frequencies where the length of the shorted stub is an odd multiple of $\lambda_{\text{eff}}/4$, where λ_{eff} is the effective wavelength of the transmission line at f_0. For this condition, low radiation occurs. On the contrary, when the length d is a multiple of $\lambda_{\text{eff}}/2$, the impedance seen from the terminated arm is much lower than the slot characteristic impedance, thus almost the entire accepted power is radiated.

Another interesting property of the derived transmission line model is the possibility to quantify the portion of radiated power that is associated with the feed point and the terminations of the slot, $P_{\text{rad},\delta}$ and $P_{\text{rad,end}}$, respectively. Figure 19 shows the power balance of a semi-infinite (a) and a finite slot (b) in the presence of a dielectric slab. The slot parameters are $w = \lambda_0/20$, $\delta = \lambda_0/40$, $h = \lambda_d/20$ and $\varepsilon_r = 4$ for both cases. In Fig. 19(a), the distance between the feeding gap and the end point is $d = \lambda_{\text{eff}}/4$ and the generator impedance is equal to $Z_{\text{gen}} = 100\Omega$. The length of the slot in Fig. 19(b) is $l = \lambda_{\text{eff}}/2$ and the generator impedance is equal to $Z_{\text{gen}} = 300\Omega$.

It can be seen that, for the semi-infinite slot in 19(a), the radiated power emerges in approximately equal parts from the feed and the end point, independently on the length of the stub. A different condition occurs in the case of a finite slot, in Fig. 19(b), for which most of the power is radiated from the terminations, when the slot length is resonant ($l = \lambda_{\text{eff}}/2$). This observation suggests that, since the semi-infinite slot is non-resonant, the radiation appears to emerge equally from the feed and the termination. Such a property is also exploited in connected arrays of slots [18], which consist of long slots periodically fed at multiple points to achieve wideband performance. Also in this case, because of the non-resonant property, the power is radiated evenly from all the feeding gaps of the array, effectively generating a uniform field distribution over the antenna aperture.

The resonant slot exhibits an opposite behavior, where the terminations have a dominant contribution to radiation compared to the feeding gaps. Indeed, in this condition, the currents are low at the feed location and very high at the end points.

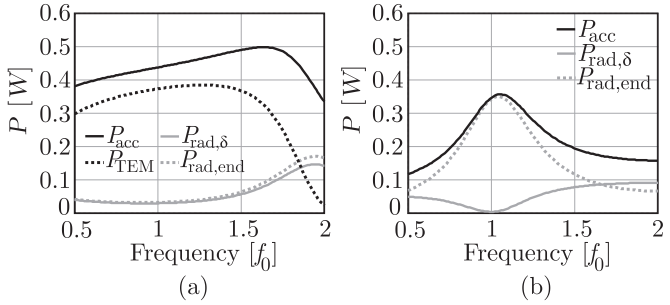

Fig. 19. Power balance of a (a) semi-infinite slot with $d = \lambda_{\rm eff}/4$ and $Z_{\rm gen} = 100\Omega$. (b) finite slot with $l = \lambda_{\rm eff}/2$ and $Z_{\rm gen} = 300\Omega$. The slots are printed on a dielectric substrate. The remaining geometrical parameters are $w = \lambda_0/20$, $\delta = \lambda_0/40$, $h = \lambda_d/20$ and $\varepsilon_r = 4$.

V. Conclusions

An equivalent transmission line model for planar slots embedded in generic stratified media was presented. The procedure started with deriving an efficient method of moments solution for semi-infinite slots, with only two basis functions, one located at the feeding point and one at the termination of the slot. The basis functions were chosen such that they properly account for the reactive energy localized at these points. The procedure was then extended to a double termination, as to find the input impedance of a finite slot antenna with arbitrary length.

Based on the numerical solution, an equivalent transmission line circuit was derived, by extraction of the pole contribution from the mutual impedance integrals. To be able to separate the residue contribution from the space wave, a thin dielectric slab or losses in the metal can be introduced. The radiation is described in the model as resistances located at the feed and the end points. This approach allows representing the radiation from the slot as the generation of different space waves, one associated with the feeding gap and two emerging from the end points. The physical dimensions and the shape of the basis functions was accounted for in the circuit by means of transformers.

References

[1] C. A. Balanis, *Antenna Theory: Analysis and Design, 4th Ed.* John Wiley & Sons, Inc., Hoboken, New Jersey, 2016.

[2] N. Behdad and K. Sarabandi, "Dual-band reconfigurable antenna with a very wide tunability range," *IEEE Trans. Antennas Propag.*, vol. 54, no. 2, pp. 409-416, Feb. 2006.

[3] C. Occhiuzzi, S. Cippitelli, and G. Marrocco, "Modeling, design and experimentation of wearable RFID sensor tag," *IEEE Trans. Antennas Propag.*, vol. 58, no. 8, pp. 2490-2498, Aug. 2010.

[4] Y. Wang and S. Chung, "A short open-end slot antenna with equivalent circuit analysis," *IEEE Trans. Antennas Propag.*, vol. 58, no. 5, pp. 1771-1775, May 2010.

[5] S. B. Cohn, "Slot line on a dielectric substrate," *IEEE Trans. Microw. Theory Tech.*, vol. 17, no. 10, pp. 768-778, Oct. 1969.

[6] R. Garg and K. C. Gupta, "Expressions for wavelength and impedance of a slotline," *IEEE Trans. Microw. Theory Tech.*, vol. 24, no. 8, pp. 532-532, Aug. 1976.

[7] J. J. Lee, "Slotline impedance," *IEEE Trans. Microw. Theory Tech.*, vol. 39, no. 4, pp. 666-672, Apr. 1991.

[8] J. Svačina, "Dispersion characteristics of multilayered slotlines — A simple approach," *IEEE Trans. Microw. Theory Tech.*, vol. 47, no. 9, pp. 1826-1829, Sep. 1999.

[9] M. Himdi and J. P. Daniel, "Analysis of printed linear slot antenna using lossy transmission line model," *Electronic letters*, vol. 28, no. 6, pp. 598-601, Mar. 1992.

[10] R. Garg, P. Bhartia, I. Bahl, and A. Ittipiboon, *Microstrip Antenna Design Handbook.* Norwood, MA, USA: Artech House, Inc., 2001.

[11] J. E. Ruyle and J. T. Bernhard, "A wideband transmission line model for a slot antenna," *IEEE Trans. Antennas Propag.*, vol. 61, no. 3, pp. 1407-1410, Mar. 2013.

[12] A. Neto and S. Maci, "Green's function for an infinite slot printed between two homogeneous dielectrics. Part I: Magnetic currents," *IEEE Trans. Antennas Propag.*, vol. 51, no. 7, pp. 1572-1581, Jul. 2003.

[13] D. Cavallo, W. H. Syed, and A. Neto, "Equivalent transmission line models for the analysis of edge effects in finite connected and tightly coupled arrays", *IEEE Trans. Antennas Propag.*, vol. 65, no. 4, pp. 1788-1796, Apr. 2017.

[14] S. van Berkel, A. Garufo, N. Llombart, and A. Neto, "A quasi-analytical tool for the characterization of transmission lines at high frequencies," *IEEE Antennas Propag. Mag.*, vol. 58, no. 3, pp. 82-90, Jun. 2016.

[15] D. Cavallo, A. Neto, and G. Gerini, "Analytical description and design of printed dipole arrays for wideband wide-scan applications," *IEEE Trans. Antennas Propag.*, vol. 60, no. 12, pp. 6027-6031, Dec. 2012.

[16] D. S. Jones, *Methods in Electromagnetic Wave Propagation, 2nd Ed.* IEEE Press, New York, 1994.

[17] M. Albani, A. Mazzinghi, and A. Freni, "Rigorous MoM Analysis of Finite Conductivity Effects in RLSA Antennas," *IEEE Trans. Antennas Propag.*, vol. 59, no. 11, pp. 4023-4032, Nov. 2011.

[18] A. Neto and J. J. Lee, "Ultrawide-band properties of long slot arrays," *IEEE Trans. Antennas Propag.*, vol. 54, no. 2, pp. 534-543, Feb. 2006.

Ralph van Schelven (S'18) received the B.Sc. and the M.Sc. degree (*cum laude*) in electrical engineering from the Delft University of Technology (TU Delft), Delft, The Netherlands in 2015 and 2017, respectively. During his Master's he specialized in telecommunications and sensing systems focusing on antennas and electromagnetic wave theory. Currently, he is pursuing the Ph.D. degree at the TU Delft with the Terahertz Sensing Group.

His current research interests include analytical/numerical techniques in electromagnetics, planar structures for pattern shaping, and waveguide based power combiners for mm-wave applications.

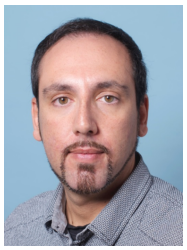

Daniele Cavallo (S'09−M'11) received the M.Sc. degree (*summa cum laude*) in telecommunication engineering from the University of Sannio, Benevento, Italy, in 2007, and his Ph.D. degree (*cum laude*) in electromagnetics from Eindhoven University of Technology (TU/e), Eindhoven, The Netherlands, in 2011.

From 2007 to 2011, he was with the Antenna Group at the Netherlands Organization for Applied Scientific Research (TNO), The Hague, The Netherlands. From 2012 to 2015, he was Post-Doctoral researcher in the Microelectronics department of TU Delft, Delft, The Netherlands. In 2015, he was a visiting researcher at Chalmers University of Technology in Gothenburg, Sweden. He currently is an assistant professor in the Terahertz Sensing Group at TU Delft. He is the author or co-author of about 120 papers published in peer-reviewed international journals and conference proceedings. His research interests include analytical and numerical methods for antenna characterization, the design of antenna arrays and on-chip antennas.

Dr. Cavallo was the first author of the paper awarded with the Best Innovative Paper Prize at the 30th ESA Antenna Workshop in 2008 and received the Best Paper Award in Electromagnetics and Antenna Theory at the 11th European Conference on Antennas and Propagation (EuCAP) in 2017. The Students he supervised received the Best Student Paper Award at EuCAP 2013, the Special Mention at EuCAP 2015, and the Else Kooi Prize in 2016. He has been awarded a three-year personal grant from the Netherlands Organization for Scientific Research (NWO VENI, 250 keuro), for developing "Efficient On-Chip Antennas for Terahertz Applications". He is currently an Associate Editor of the IEEE TRANSACTIONS ON ANTENNAS AND PROPAGATION.

Andrea Neto (M'00−SM'10−F'16) received the Laurea degree (*summa cum laude*) in electronic engineering from the University of Florence, Florence, Italy, in 1994, and the Ph.D. degree in electromagnetics from the University of Siena, Siena, Italy, in 2000. Part of his Ph.D. degree was developed at the European Space Agency Research and Technology Center, Noordwijk, The Netherlands.

He was with the Antenna Section, European Space Agency Research and Technology Center for over two years. From 2000 to 2001, he was a Post-Doctoral Researcher with the California Institute of Technology, Pasadena, CA, USA, where he was with the Sub-Millimeter-Wave Advanced Technology Group. From 2002 to 2010, he was a Senior Antenna Scientist with TNO Defense, Security, and Safety, The Hague, The Netherlands. In 2010, he became a Full Professor of applied electromagnetism with the EEMCS Department, Technical University of Delft, Delft, The Netherlands, where he formed and leads the Terahertz Sensing Group. His current research interests include the analysis and design of antennas with an emphasis on arrays, dielectric lens antennas, wideband antennas, EBG structures, and terahertz antennas.

Dr. Neto served as an Associate Editor of the IEEE TRANSACTIONS ON ANTENNAS AND PROPAGATION from 2008 to 2013 and the IEEE ANTENNAS AND WIRELESS PROPAGATION LETTERS from 2005 to 2013. He is a member of the Technical Board of the European School of Antennas and an organizer of the course on antenna imaging techniques. He is a member of the steering committee of the Network of Excellence NEWFOCUS, dedicated to focusing techniques in mm and sub-millimeter-wave regimes. In 2011, he was a recipient of the European Research Council Starting Grant to perform research on Advanced Antenna Architectures for THz Sensing Systems, the H. A. Wheeler Award for the best applications paper of 2008 in the IEEE TRANSACTIONS ON ANTENNAS AND PROPAGATION, the Best Innovative Paper Prize of the 30th ESA Antenna Workshop in 2008, the Best Antenna Theory Paper Prize at the European Conference on Antennas and Propagation (EuCAP) in 2010.